Capillarity-Induced Patterning of Thin Polymer Films and Related Regular Dewetting Structures

KAHP Y. SUH

School of Mechanical and Aerospace Engineering, Seoul National University, Seoul, 151-742, Korea

Abstract. When a thin polymer film is spin-coated on a solid substrate and heated above its glass transition temperature (T_g) while in conformal contact with a patterned polydimethylsiloxane (PDMS) mold, capillarity forces the polymer melt to fill up the void space of the mold, thereby forming a negative replica of the polymer after mold removal. In this study, particular emphasis is given to the nodal dewetting phenomenon in a thin, laterally confined polymer film that sticks to a substrate. When heated above the glass transition temperature, the film dewets from the substrate through the generation of nodal waves, with the PDMS wall acting as a node. Various superposed waves were observed depending on the intrinsic period of dewetting and the confining width of the cavity.

1. INTRODUCTION

Recently, structure formation and thermal stability of thin liquid films on partially wetted substrates have attracted much attention due to fundamental interest in basic wetting phenomena and applications to nano-patterning technology.[1–5] Until now, most studies have been devoted to the dewetting behavior of two-dimensional polymer films. These studies revealed that there are two classical dewetting routes in the thin films: a process whereby film rupture is induced by nucleated holes,[6] and a different pathway through which van der Waals intermolecular forces amplify thermal fluctuations (often termed "spinodal dewetting").[7]

It has been reported that the spinodal dewetting takes hold for very thin films of polymer (typically <10 nm) of low molecular weight (<10^4).[7] On the other hand, nucleation of holes takes place for intermediate film thickness (100 nm to 1μm), which is accelerated by the presence of small particles (i.e., dust) or imperfections on the surface.[8]

Our dewetting experiment presented here is based on a new lithographic technique called capillary force lithography (CFL),[9] which was recently developed for patterning polymers on a large area. When a patterned polydimethylsiloxane (PDMS) mold is in place on a spin-coated polymer film and then heated above the glass transition temperature (T_g), the capillarity forces the polymer melt into the void space of the mold, thus forming a negative replica after mold removal. CFL is a high-temperature process and thus under certain conditions generates an ordered, dewetting structure within the cavity[10,11] or around the protruding feature in contact with the polymer surface.[12,13] A schematic diagram for
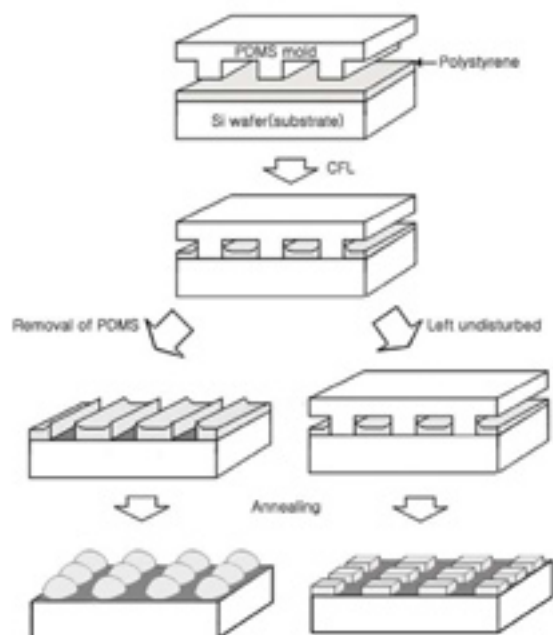
E-mail: sky4u@snu.ac.kr

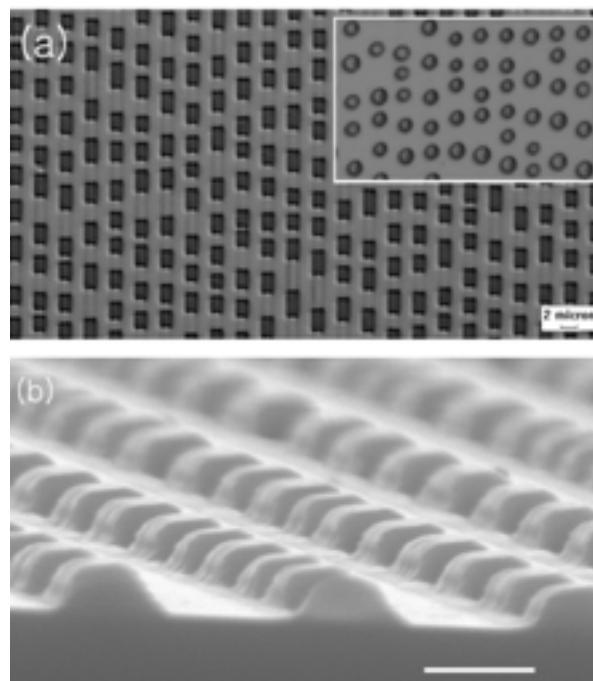Fig. 1. A schematic diagram of the experimental procedure for typical dewetting experiments.

Fig. 2. (a) An optical image of separated blocks of 1.5-μm-wide polymer strips that resulted when confined by PDMS walls. The inset shows separated drop formation in the same strips that are not confined by PDMS walls. (b) An SEM cross-sectional view of (a). The scale bar represents 1.5 μm. The initial thickness is 70 nm and the samples were annealed at 160 ℃.

the formation of dewetting structures is shown in Fig. 1. With the polymer strips formed by CFL, annealing can be carried out in two different ways. In one, the whole structure was left undisturbed at the chosen heating temperature in air with the mold in place. After a period of time, the PDMS mold was removed after cooling to room temperature. In the other, the PDMS mold was removed at room temperature after forming polymer strips (channels) and then the strips were annealed at the chosen heating temperature. Regularly spaced, distinctly observable polymer structures have been obtained using this approach.[10–13] A typical example is shown in Fig. 2 using polystyrene (PS) (molecular weight = 24.7k, T_g = 100 ℃). In general, the droplet formation process in the absence of the walls is much different than that with confining PDMS walls in terms of the final shape of the fragments and transient morphology (drops vs. blocks).[11] However, the period of the drops and that of the blocks are about the same whether confined or unconfined. This similarity in the wavelength strongly indicates that the same Rayleigh instability governs the rupture process.

In this work, we report on a new dewetting pathway of a thin polymer film that sticks to a substrate. The confinement gives rise to the formation of nodal waves, with the walls providing the nodes, and thus the dewetting can be termed "nodal dewetting".

Au: 24.7 kDa?

2. EXPERIMENTAL
For the experimental setup, we fabricated a PDMS (Sylgard 184, Dow Corning) mold that has a planar surface with recessed patterns by casting PDMS against a complementary relief structure prepared by the photolithographic method.[14] The mold has a line-and-space pattern with the lines varying in width from 1 to 3 μm and a step height of 550 nm. The mold with the pattern is placed on the surface of a polymer layer spin-coated onto hydrogen-terminated substrates and then heated well above the glass transition temperature of the polymer (typically 130~150 ℃). In order to prepare a clean, H-terminated surface, we dipped the silicon wafer into pirana solution (H_2SO_4:H_2O_2 = 4:1) for 20 minutes and then dipped into 10 wt% HF solution. For the polymer, we used commercial polystyrene (PS) (molecular weight = 2.3 × 10^5, T_g = 101 ℃, Aldrich). It should be noted that the high molecular weight used in our experiment is a prerequisite for the observation of nodal dewetting. A polymer film was spin-coated onto the substrate to 30 nm to 90 nm thickness as confirmed by ellipsometry, and the resulting structure was examined by atomic force microscopy (AFM) operated in the contact mode.
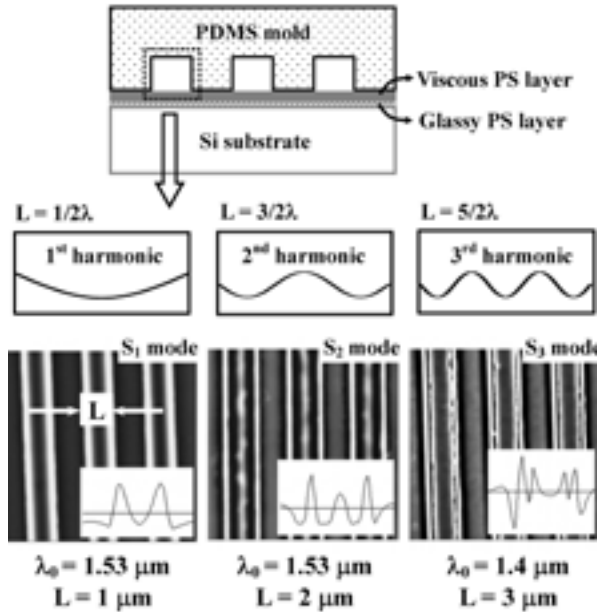
Fig. 3. A schematic diagram of the experimental setup for nodal dewetting presented in this study.

3. RESULTS AND DISCUSSION

Figure 3 shows three harmonics that can be generated by the nodal condition along with the relationship between the channel width L and the wavelength λ. Also shown are three types of superposed modes that are observed experimentally in microcavities. In contrast to the conventional standing wave problem, the nodal dewetting presented here is always accompanied by wetting at the wall such that all the nodal waves are superposed with wetting-induced first harmonic. For convenience, we refer to each nodal pattern as S_i (i = 1,2,3…), depending on the number of harmonic waves superposed. For example, S_2 mode is the mode resulting from the superposition of two waves and S_3 mode, the superposition of three waves.

When there are no special interactions at the film–substrate interface (absence of a glassy layer), the fundamental harmonic is typically observed, which is associated with meniscus formation within the channel. A previous study for this case revealed that the minimum meniscus height could keep decreasing as the meniscus develops and this meniscus-induced reduction in the film thickness can cause instability across the channel that leads to a breakdown of meniscus due to film–substrate interactions.[15] However, the second and third superposed modes (S_2 and S_3) cannot be understood on the basis of simple meniscus formation, for which nodal waves are responsible.

In the nodal dewetting, the line width L is related to the wavelength λ by

$$L = \frac{2n-1}{2}\lambda \quad (n = 1, 2, 3...) \quad (1)$$

It is of interest to find how this wavelength imposed by the nodal condition compares with the intrinsic wavelength λ_0, which results in the absence of the confinement. To begin with, the first harmonic is always present in the superposed wave due to the wetting at the walls. There are also two extremes one can envision. In one extreme, the channel width can be much smaller than the intrinsic wavelength. Then, only the capillary rise takes place and thus a simple meniscus is generated, which is a form of fundamental harmonic. In the other extreme, the channel width can be much larger than the intrinsic period. In such a case, practically no confinement effects are present, and thus the wavelength is that corresponding to the intrinsic wavelength. In fact, we found for the system under consideration that the confinement effects are absent when the channel width is larger than 5 μm for the film thickness used in our experiment. Between these two extremes lies the range in which the superposition of waves takes place. Since the system tries to maintain its intrinsic wavelength, the harmonic whose wavelength is the closest to the intrinsic value dominates, as will be shown shortly, when it reaches equilibrium. For the second superposed mode, S_2 in Fig. 3, the wavelength of the first harmonic is 4 μm and that of the second harmonic is 1.33 μm, the latter of which is closer to the intrinsic wavelength of 1.53 μm. Therefore, the S_2 mode is the result of superposition of the first and second harmonics, which is dominated by the second harmonic at equilibrium. For the S_3 mode in the figure, the intrinsic wavelength is 1.4 μm and the periods of the second and third harmonics are 2 and 1.2 μm, respectively. Therefore, the S_3 mode is the mode resulting from the superposition of the first, second, and third harmonics with the major contribution coming from the third harmonic.

The intrinsic wavelength of dewetting for the unconfined system was determined experimentally on the basis of fast Fourier transform (FFT). We found that the intrinsic period of dewetting is nearly independent of film thickness such that it ranges between 1.3 and 1.5 μm for hydrogen-terminated silicon substrate. For strongly confined polymer systems such as polystyrene (PS) on hydrogen-terminated Si and polyvinyl pyridine (PVP) on SiO_2,[16–18] the conventional capillary wave model fails to explain the dewetting behavior and a new model is needed to take into account the built-in thermal stress generated at the polymer–substrate interface due to an immobile glassy layer.[19]
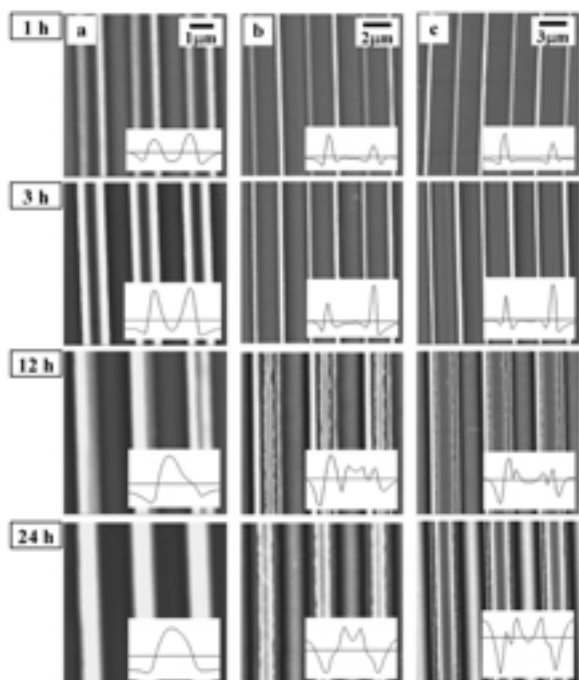
Fig. 4. Two-dimensional and cross-sectional AFM micrographs for the temporal progression of nodal dewetting for 1 (a), 2 (b), and 3 μm (c) line-and-space pattern as a function of annealing time (1, 3, 12, and 24 h). Note that the height profile is a linear combination of two to three harmonics. Also note that the overall curvature changes from concave to convex shape as the annealing time increases.
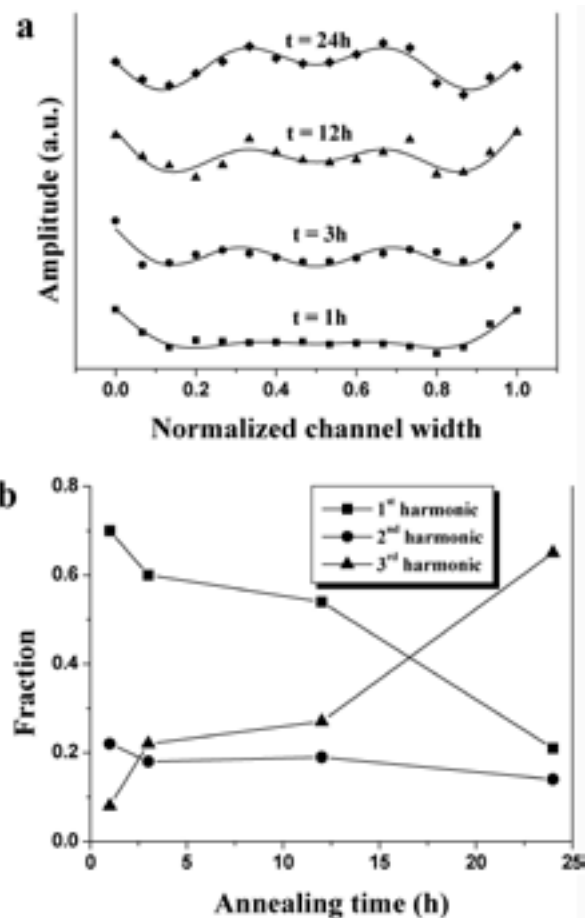

Fig. 5. (a) Representation of the superposed waves in Fig. 4 with a linear combination of three harmonics for 3-μm pattern. The symbols are for the experimental AFM profiles and the solid lines represent the superposed waves. (b) Change of the fractions of the three harmonics with annealing time.

Figure 4 shows temporal progression of morphologies of the nodal patterns (1, 3, 12, and 24 h) for 1 (a), 2 (b), and 3 μm (c) line-and-space pattern. In the initial annealing stage, concave waves are observed for all the channel widths because of the major contribution from the first harmonic and the acute contact angle at the PS/PDMS interface ($\theta_{real} \sim 70°$).[15] Experimental results in Fig. 4 show that the concave shapes persist until the annealing time reaches 12 h. However, convex shapes start appearing as the annealing time increases further such that a complete inversion of the curvature takes place after annealing for 24 h. As discussed below, the curvature inversion is related to increasing contribution from higher harmonics with time.

To examine the wave superposition in more detail, we fit the cross-sectional profiles for the 3-μm pattern in Fig. 4 as a linear combination of three harmonics in Fig. 5a. As the intrinsic wavelength here is 1.4 μm, it is expected that the shape can be determined by the wave superposition of three harmonics. For convenience, we normalized the channel axis with respect to the channel width (L), which gives the height profile (h) as

$$h = \sum_{n=1}^{4} f_n (-1)^n \cos[(2n-1)\pi(x-0.5)]$$

where f_n is the fractional contribution from the nth harmonic and x is the normalized channel axis. The change of these three fractions with time is shown in Fig. 5b. As shown in the figure, all the three harmonics are present initially as the polymer wets the mold. This fact reveals that the wetting at the PS/PDMS interface is an important step for the initial wave superposition. As the annealing time increases, however, the fractions for the first and second harmonics keep decreasing, whereas the contribution from the third harmonic keeps increasing up to 65% after annealing 1 day. No further change was observed after 1 day such that the system can be

Au: Changed from "shortly".

considered to have reached equilibrium after 1 day. The intrinsic wavelength is 1.4 μm, which is closest to the wavelength of the third harmonic. Therefore, the S_3 mode in this case consists of three harmonics with the third harmonic contributing the most to the superposed wave eventually. The contributions from the higher harmonics are responsible for the inversion of the curvature. The concave shape maintained in the initial annealing stage up to 12 h inverts to the convex shape as the major contribution from the third harmonic asserts itself with time.

4. CONCLUSIONS

Capillarity-induced patterning is an alternative method for fabricating polymeric micro/nanostructures over a large area. During the annealing process, a metastable polymer film can dewet from the substrate, resulting in various regular dewetting structures inside or outside the cavity that is formed between the PDMS mold and the substrate surface. Of these dewetting structures, the nodal dewetting pathway was examined in this work using a thin polymer film that sticks to a solid substrate.

Our findings can be summarized into two aspects. First, three types of superposed waves were observed depending on the intrinsic wavelength of dewetting and the confining width of cavity. In the absence of special interactions at the film–substrate interface, the fundamental harmonic (S_1) was typically observed, the formation of which was attributed to meniscus formation within the channel. When the channel width is relatively large with respect to that of the intrinsic wavelength, two superposed modes (S_2 and S_3) were formed instead of a simple meniscus. Second, the cross-sectional profile of the polymer front can be given by a superposition of three nodal modes. Depending on the fraction of each mode, a concave or convex curvature was observed.

Since this method can form a specific shape of the meniscus by controlling the intrinsic period and the confining width, it can provide a new route to shape engineering of the polymer surface through self-organization. Also, the period of the structure can be further reduced from the original width of the mold, which is advantageous for micro/nanofabrication. More funda-mentally, the method presented here would offer a useful tool for studying wetting/dewetting behavior of a thin polymer film under a confined geometry.

REFERENCES AND NOTES

(1) Yerushalmi-Rozen, R.; Kerle, T.; Klein, J. *Science* **1999**, *285*, 1254.

(2) Herminghaus, S.; Jacobs, K.; Mecke, K.; Bischof, J.; Fery, A.; Ibn-Elhaj, M.; Schlagowski, S. *Science*, **1998**, *282*, 916.

(3) de Crevoisier, G.; Fabre, P.; Corpart, J.M.; Leibler, L. *Science* **1999**, *285*, 1246.

(4) Higgins, A.M.; Jones, R.A.L. *Nature* **2000**, *404*, 476.

(5) Gleiche, M.; Chi, L.F.; Fuchs, H. *Nature*, **2000**, *403*, 173.

(6) Reiter, G. *Phys. Rev. Lett.* **1992**, *68*, 75.

(7) Xie, R.; Karim, A.; Douglas, J.F.; Han, C.C.; Weiss, R.A. *Phys. Rev. Lett.* **1998**, *81*, 1251.

(8) Leger, L.; Joanny, J. F. *Rep. Prog. Phys.* **1992**, *55*, 431.

(9) Suh, K.Y.; Kim, Y.S.; Lee, H.H. *Adv. Mater.* **2001**, *13*, 1386.

(10) Xia, Y.N.; Rogers, J.A.; Paul, K.E.; Whitesides, G.M. *Chem. Rev.* **1999**, *99*, 1823.

(11) Suh, K.Y.; Lee, H.H. *J. Chem. Phys.* **2001**, *115*, 8204.

(12) Park, J.Y.; Suh, K.Y.; Seo, S.M.; Lee, H.H. *J. Chem. Phys.* **2006**, *124*, 214710.

(13) Suh, K.Y.; Park, J.; Lee, H.H. *J. Chem. Phys.* **2002**, *116*, 7714.

(14) Suh, K.Y.; Seo, S.M.; Yoo, P.J.; Lee, H.H. *J. Chem. Phys.* **2006**, *124*, 024710.

(15) Suh, K.Y.; Yoo, P.J.; Lee, H.H. *Macromolecules* **2002**, *35*, 4414.

(16) Wang J.; Tolan, M.; Seeck, O.H.; Sinha, S.K.; Bahr, O.; Rafailovich, M.H.; Sokolov, J. *Phys. Rev. Lett.* **1999**, *83*, 564.

(17) Wallace, W.E.; van Zanten, J.H.; Wu, W.L. *Phys. Rev. E* **1995**, *52*, R3329.

(18) van Zanten, J.H.; Wallace, W.E.; Wu, W.L. *Phys. Rev. E* **1996**, *53*, R2053.

(19) Suh, K.Y.; Lee, H.H. *Phys. Rev. Lett.* **2001**, *87*, 135502.